Indian Journal of Pure & Applied Physics
Vol. 59, January 2021, pp. 48-62

Structural, spectroscopic, electronic, and nonlinear optical behavior investigations of π conjugated organic nonlinear optical chalcone derivative 3-(2,3-dichlorophenyl)-1-(pyridine-2-yl)prop-2-en-1-one using DFT

Varsha Rani, Akansha Tyagi & Anuj Kumar*

Department of Physics, Chaudhary Charan Singh University, Meerut-250 004, Uttar Pradesh, India

Received 18 June 2020; accepted 15 October 2020

In this paper, we have reported the computational studies of structural, spectroscopicand electronic behavior of a chalcone derivative:3-(2,3- dichlorophenyl)-1-(pyridine-2- yl)prop-2-en-1-one (DCPP) nonlinear optical crystal. The geometry of DCPP molecule have been optimized using density functional theory (DFT) at B3LYP level having extended basis set 6-311++G(d,p) with the help of Gaussian 09W program package. Taking this optimized geometry FTIR spectrum was simulated and analyzed quantitatively with the help of calculated potential energy distribution (PED). For finding the reactivity sites and to understand electronic and optical behavior, natural bond orbital (NBO), the electrostatic potential surface map with isodensity surface, and HOMO-LUMO analysis were also presented. Finally, the nonlinear optical behavior of this chalcone derivative was studied by calculating dipole moment (μ), polarizability (α) and hyperpolarizability (β) values. The calculated hyperpolarizability β_{tot} of DCPP is 17.4593×10^{-30}esu which is about 90 times greater than urea ($\beta= 0.1947\times 10^{-30}$ esu). This higher value of hyperpolarizability β_{tot} confirms that the present molecule DCPP is a potential candidate for Nonlinear Optical applications.

Keywords: Nonlinear optical crystal, DFT, Natural bond orbital analysis, HOMO-LUMO, Hyperpolarizability.

1 Introduction

In last two decades, organic nonlinear optical (NLO) materials have found wide research interest due to easy design and their large optical nonlinearities. These materials have potential applications in photonics and optoelectronics; like optical communication, harmonic generation, dynamic holography, optical switching and optical limiting *etc*.[1,2] A special class of organic NLO materials with cross conjugated chromophores, known as Chalcones, have been studied extensively because of their good SHG efficiency, transparency, better optical limiting behavior and ultrafast optical nonlinearities[3-6]. It was suggested by Wu *et al.*[7] that the presence of carbonyl group in the middle splits the conjugated system in to two independent parts making these molecules cross conjugated[7]. Depending upon the symmetry of their structure chalcone derivatives show both first and second order hyperpolarizabilities β and γ respectively. The nonlinear susceptibility of these derivatives are found of the order of 10^{-13}esu and very much depend upon the strength of the donor and acceptor group across the π conjugated backbone[1]. Thus by changing the donor-acceptor group can affect the nonlinear properties of chalcone derivatives up to large extent. This unique nature make the chalcone derivatives, a potential candidate for a comprehensive theoretical investigations for understanding the effect of substitution of donor-acceptor groups at microscopic level. Therefore, we have theoretically investigated many chalcone derivatives using Density Functional Theory[3,8].

In an attempt to enhance our understanding on one more chalcone derivative, we present here theoretical investigations on molecular structure, vibrational spectra and nonlinear behavior of chalcone derivative: 3-(2,3- dichlorophenyl)-1-(pyridine-2- yl)prop-2-en-1-one (DCPP) using density functional theory (DFT) method using 6-311++G(d,p) basis set and Becke's three- parameter hybrid functional (B3LYP). For the validation of our computational data we have compared our calculated results with experimental values as reported by B. Ganapayya *et al.*[6]. In this paper we report here detailed analysis of geometry optimization and vibrational spectra using DFT method with the help of Gaussian 09 program package[9]. A comparison of optimized structure and vibrational peaks calculated show excellent matching

*Corresponding author: (E-mail:dranujkumarccsu@gmail.com)

with experimental data[6]. All the vibrational modes were assigned with the help of the potential energy distribution (PED).

The electronic behavior of the molecule was analyzed by molecular electrostatic potential (MEP), natural bond orbital (NBO) analysis and highest occupied molecular orbital (HOMO) and the lowest unoccupied molecular orbital (LUMO) energy. The electronic distribution of HOMO-LUMO states were depicted using Gauss view software and was further confirmed by the determination of density of states (DOS) spectra. NBO analysis was done to understand the nature of different interactions which causes the electron delocalization and intra-molecular charge transfer which is ultimately responsible for nonlinear behavior as well as many biological activities such as anti-fungal, antibiotic *etc*. shown by the molecules. The nonlinear optical behavior of the title molecule DCPP was analyzed by total static dipole moment μ, the polarizability α and first hyper polarizability β calculations.

2 Computational Details

Structure and geometry optimization of the stable conformer of the molecule has been done by minimizing the energy with respect to all parameters without imposing any constraint on the potential energy surface using density functional theory (DFT)[10], built in Gaussian 09 program package[9].The calculations were done applying different basis sets and Becke's three-parameter hybrid functional (B3LYP)[11-13]. The stability of the optimized structures is also checked by calculating vibrational frequencies. Absence of any imaginary frequency is the indication of a true minimum on the potential energy surface. For the optimized geometry, Infrared absorption intensities have been calculated using harmonic approximation at the same functional and basis set. The normal-mode analysis was carried out to find potential energy distribution for each of the internal coordinates using no symmetry. For the calculations of PED, all internal coordinates were defined as per the recommendations by Pulay *et al.*[14-15]. The assignments of the modes were proposed on the basis of the PED obtained using the program GAR2PED[16]. Calculated DFT vibrational wave numbers are higher than the experimental wave numbers as the anharmonicity effects are neglected. To overcome this problem the obtained wave numbers from DFT calculations were scaled down by the wave number linear scaling procedure. As suggested by Maurya *et al.*[17] simple linear scaling with scaling factors of 0.9551 and 0.9768 have been used for the wave number ranges, above 2500 cm^{-1} and below 2500 cm^{-1} respectively.

3. Results and Discussion

3.1. Geometry Optimization

The geometry of DCPP molecule have been optimized using DFT at B3LYP level having extended basis sets 6-311++G(d,p), 6-311+G(d,p), and 6-311G(d,p) with the help of Gaussian 09W program package[9]. All the optimized values of bond lengths, bond angles and torsions of the DCPP molecule are arranged in Table 1. The title compound contains phenyl, pyridine and carbonyl moieties. In DCPP, Pyridine ring and phenyl ring are interconnected by a highly electrophilic ketoethylenic group (-CO-CH=CH-). Optimized geometry predicts the planner structure of the molecule. However, in experimental result, a small twisting of Pyridine ring, at N6–C5–C11–C13 by -1.5^{o} and Phenyl ring by -22.4^{0} at C13-C15-C17-C18 with enonemoity is observed. Similar differences in other torsion angles between computed values and experimental values are observed about C5-C11 and C15-C17 bonds. These minor discrepancies are incorporated because of our isolated model chosen for theoretical calculations, while experimental values involve intermolecular interactions caused by solid state of the crystal.

The accurate determination of geometrical distortions in the ring is important for investigating the nature of the interactions between the ring and the substituents. In the phenyl ring, little deviation in the bond lengths of C17-C22, C17-C18, C20-C21 and C21-C22 bonds, close to the substitution place, appear as elongation in size ((~1.40 Å) than other C-C bond lengths of phenyl rings (~1.36 Å). The angles are also slightly out of perfect hexagonal structure. These distortions can be explained in terms of the change in electron density of bonds due to the presence of electron withdrawing Chlorine atoms attached as substituent. The lengths of C-H bonds are particularly important in terms of explanation of hydrogen bonding and unlikely to change by more than 0.001 Å in the absence of hydrogen bond. The calculated C-H bond lengths in the phenyl and pyridine rings are almost equal to 1.08 Å, which are in agreement with standard data. The matching of geometrical parameters calculated at various basis sets, 6-311++G(d,p), 6-311+G(d,p) and 6-311G(d,p) are analyzed by regression coefficient analysis. The R^2

Table 1 — Optimized geometrical parameters (Bond angles and torsions) of DCPP by DFT in comparison with XRD data.

Geometrical parameters	Experimental values [6]	Optimized		
		B3LYP/ 6-311++G(d,p)	B3LYP/ 6-311+G(d,p)	B3LYP/ 6-311G(d,p)
Cl27-C22	1.734	1.744	1.744	1.744
Cl26-C21	1.729	1.749	1.749	1.750
O12-C11	1.212	1.222	1.230	1.221
N6-C1	1.323	1.333	1.336	1.333
N6-C5	1.340	1.340	1.344	1.339
C1-H7	0.930	1.086	1.087	1.086
C1-C2	1.374	1.394	1.398	1.396
C2-H8	0.930	1.083	1.085	1.083
C2-C3	1.365	1.393	1.396	1.392
C3-H9	0.930	1.084	1.086	1.084
C3-C4	1.380	1.389	1.392	1.388
C4-H10	0.930	1.082	1.084	1.081
C4-C5	1.378	1.398	1.401	1.398
C5-C11	1.496	1.511	1.510	1.510
C11-C13	1.473	1.483	1.483	1.483
C13-H14	0.930	1.075	1.077	1.075
C13-C15	1.312	1.346	1.350	1.344
C15-H16	0.930	1.088	1.089	1.088
C15-C17	1.473	1.464	1.466	1.464
C17-C18	1.395	1.409	1.412	1.409
C17-C22	1.405	1.416	1.419	1.415
C18-H23	0.930	1.083	1.085	1.083
C18-C19	1.383	1.385	1.389	1.384
C19-H24	0.930	1.083	1.085	1.083
C19-C20	1.366	1.389	1.392	1.388
C20-H25	0.930	1.082	1.084	1.081
C20-C21	1.380	1.392	1.396	1.391
C21-C22	1.364	1.400	1.404	1.400
C1-N6-C5	116.3	117.0	117.9	117.9
N6-C1-H7	117.4	116.2	116.1	116.1
N6-C1-C2	125.1	123.2	123.3	123.2
H7-C1-C2	117.5	120.5	120.5	120.5
C1-C2-H8	121.2	120.1	120.1	120.1
C1-C2-C3	117.7	118.4	118.4	118.5
H8-C2-C3	121.1	121.3	121.3	121.2
C2-C3-H9	120.4	120.6	120.6	120.6
C2-C3-C4	119.3	118.7	118.7	118.7
H9-C3-C4	120.4	120.5	120.5	120.6
C3-C4-H10	120.7	122.3	122.3	122.5
C3-C4-C5	118.7	118.5	118.5	118.5
H10-C4-C5	120.6	119.0	119.0	118.8
N6-C5-C4	123.0	122.9	122.9	123.0
N6-C5-C11	116.3	118.0	117.9	118.0
C4-C5-C11	120.7	119.0	119.0	118.9
O12-C11-C5	120.5	119.5	119.4	119.6
O12-C11-C13	121.7	123.3	123.2	123.3
C5-C11-C13	117.8	117.0	117.3	117.0
C11-C13-H14	118.8	116.6	116.7	116.5
C11-C13-C15	122.3	118.7	118.6	118.5
H14-C13-C15	118.9	124.6	124.5	124.8
C13-C15-H16	116.5	114.4	114.3	114.2
C13-C15-C17	126.8	132.8	132.8	132.9
H16-C15-C17	116.6	112.6	112.7	112.7

(*Contd*.)

Table 1 — Optimized geometrical parameters (Bond angles and torsions) of DCPP by DFT in comparison with XRD data. (*Contd*.)

Geometrical parameters	Experimental values [6]	Optimized		
		B3LYP/ 6-311++G(d,p)	B3LYP/ 6-311+G(d,p)	B3LYP/ 6-311G(d,p)
C15-C17-C18	120.4	114.9	114.9	115.0
C15-C17-C22	121.6	127.9	127.9	127.9
C18-C17-C22	118.0	117.0	117.0	117.0
C17-C118-H23	120.0	117.9	117.9	117.8
C17-C18-C19	120.0	122.4	122.4	122.4
H23-C18-C19	120.0	119.6	119.5	119.6
C18-C19-H24	119.4	120.3	120.3	120.3
C18-C19-C20	121.3	119.7	119.6	119.6
H24-C19-C20	119.3	119.9	119.9	119.9
C19-C20-H25	120.5	121.2	121.2	121.3
C19-C20-C21	119.1	119.5	119.5	119.5
H25-C20-C21	120.4	119.2	119.2	119.1
Cl26-C21-C20	118.1	117.6	117.6	117.6
Cl26-C21-C22	121.0	121.2	121.2	121.3
Cl27-C21-C22	120.9	121.0	121.0	121.0
Cl27-C22-C17	119.1	121.5	121.5	121.5
Cl27-C22-C21	120.2	118.2	118.3	118.3
C17-C22-C21	120.7	120.1	120.1	120.1
C5-N6-C1-H7	-178.4	180.0	-180.0	180.0
C5-N6-C1-C2	1.7	0.0	0.0	-0.00054
C1-N6-C5-C4	-1.3	0.0	0.0	0.00042
C1-N6-C5-C11	178.7	180.0	-180.0	-179.99
N6-C1-C2-H8	178.6	180.0	180.0	-179.99
N6-C1-C2-C3	-1.4	0.0	0.0	0.00026
H7-C1-C2-H8	-1.3	0.0	0.0	0.0
H7-C1-C2-C3	178.6	-180.0	-180.0	180.0
C1-C2-C3-H9	-179.2	-180.0	-180.0	-179.99
C1-C2-C3-C4	0.8	0.0	0.0	0.0
H8-C2-C3-H9	0.8	0.0	0.0	0.00040
H8-C2-C3-C4	-179.3	-180.0	-180.0	-180.0
C2-C3-C4-H10	179.5	-180.0	-180.0	179.99
C2-C3-C4-C5	-0.5	0.0	0.0	-0.00027
H9-C3-C4-H10	-0.5	0.0	0.0	-0.00095
H9-C3-C4-C5	179.5	180.0	-180.0	179.99
C3-C4-C5-N6	0.8	0.0	0.0	0.0
C3-C4-C5-C11	-179.3	-180.0	180.0	180.0
H10-C4-C5-N6	-179.2	180.0	180.0	-179.99
H10-C4-C5-C11	0.8	0.0	0.0	0.0
N6-C5-C11-O12	178.6	-180.0	-179.99	179.99
N6-C5-C11-C13	-1.5	0.0	0.0	-0.00271
C4-C5-C11-O12	-1.4	0.0	0.0011	-0.00263
C4-C5-C11-C13	178.5	-180.0	180.0	179.99
O12-C11-C13-H14	166.4	180.0	179.99	179.99
O12-C11-C13-C15	-13.6	0.0	0.0	0.0
C5-C11-C13-H14	-13.6	0.0	0.00080	-0.00042
C5-C11-C13-C15	166.4	-180.0	-179.99	179.99
C11-C13-C15-H16	1.9	0.0	0.00027	0.00094
C11-C13-C15-C17	-178.1	-180.0	179.99	179.99
H14-C13-C15-H16	-178.0	-180.0	-179.99	-179.99
H14-C13-C15-C17	2.0	0.0	-0.00039	-0.00194
C13-C15-C17-C18	-22.4	-179.99	-179.99	-179.98
C13-C15-C17-C22	157.7	0.0094	0.0057	0.0127
H16-C15-C17-C18	157.5	0.01002	0.00461	0.00790
H16-C15-C17-C22	-22.3	-179.98	-179.98	-179.99
C15-C17-C18-H23	-0.1	0.0	0.0	-180.0

(*Contd*.)

Table 1 — Optimized geometrical parameters (Bond angles and torsions) of DCPP by DFT in comparison with XRD data. (*Contd*.)

Geometrical parameters	Experimental values [6]	Optimized		
		B3LYP/ 6-311++G(d,p)	B3LYP/ 6-311+G(d,p)	B3LYP/ 6-311G(d,p)
C15-C17-C18-C19	179.9	180.0	179.99	0.00066
C22-C17-C18-H23	179.7	180.0	179.99	179.99
C22-C17-C18-C19	-0.2	0.0	-0.00057	-0.00097
C15-C17-C22-Cl27	-0.3	0.0	0.00078	-0.00029
C15-C17-C22-C21	-179.2	-180.0	-179.99	179.99
C18-C17-C22-Cl27	179.8	180.0	-179.99	-179.99
C18-C17-C22-C21	1.0	0.0	0.00042	0.0
C17-C18-C19-H24	-179.9	-180.0	-180.0	-179.99
C17-C18-C19-C20	0.1	0.0	0.0003	0.00119
H23-C18-C19-H24	0.1	0.0	0.0	0.00040
H23-C18-C19-C20	-179.9	180.0	-180.0	-179.99
C18-C19-C20-H25	179.4	180.0	180.0	179.99
C18-C19-C20-C21	-0.6	0.0	0.0	-0.00034
H24-C19-C20-H25	-0.6	0.0	0.0	-0.00062
H24-C19-C20-C21	179.4	180.0	-180.0	-180.0
C19-C20-C21-Cl26	-178.6	180.0	179.99	179.99
C19-C20-C21-C22	1.4	0.0	0.0	-0.00067
H25-C20-C21-Cl26	1.4	0.0	0.0	0.0
H25-C20-C21-C22	-178.6	-180.0	180.0	180.0
Cl26-C21-C22-Cl27	-0.4	0.0	-0.00041	0.0
Cl26-C21-C22-C17	178.4	180.0	-180.0	-179.99
C20-C21-C22-Cl27	179.6	180.0	179.99	180.0
C20-C21-C22-C17	-1.6	0.0	0.0	0.00088

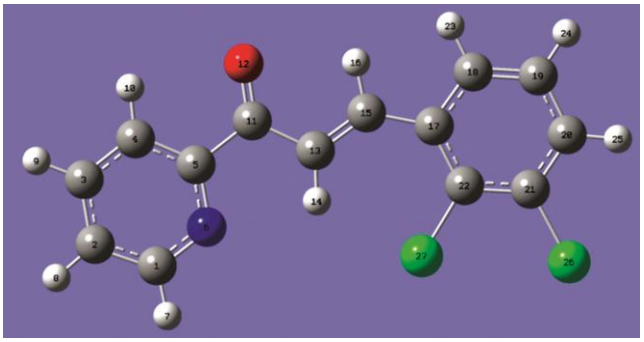

Fig. 1 — Optimized Structure of DCPP at the B3LYP/6-311++G (d,p) level of theory.

value is calculated equal to 0.99, 0.71 and 0.70 respectively for 6-311++G(d,p), 6-311+G(d,p) and 6-311G(d,p) basis sets. This confirms that computed geometry at B3LYP/6-311++G(d,p) shows excellent matching with the experimental results. Therefore, geometry optimized at 6-311++G (d,p) basis set is shown in Fig. 1 and will be used for further computations.

3.2. Infrared Spectroscopy

Title DCPP molecule is made of 27 atoms that gives (3n-6) = 75 normal modes. Detailed assignments of vibrational modes are made using PED calculations. Table 2 shows the potential energy distribution of each vibrational mode in terms of percentage contribution coming from various vibrational motions calculated at B3LYP/6-311++G(d,p) level of theory. Theoretically calculated harmonic wave numbers are higher due to neglected anharmonicity terms and scaled down as discussed in computational details section. A satisfactory matching is found between theoretical (scaled) and experimental spectrum[6] peaks. In experimental FTIR spectrum, peaks are assigned on the basis of relative intensities, line shape and literature review[3,6, 8].

A pictorial comparison of computed FTIR spectra with experimental spectrum[6] is shown in Fig. 2. As visible from Fig. 2, a satisfactory matching between theoretical and experimental spectra is observed, this further validate the choice of the basis set used.

For the better understanding, important vibrational modes have been analyzed by dividing them into different groups which are given below.

3.2.1 Pyridine Ring (Ring 1) Vibrations

The Pyridine ring has CH, C-C and C-N vibrations. CH stretching vibrations in Pyridine ring are mainly confined in the range 3029-3091 cm^{-1} and generally do not mix with other vibrations[3]. In DCPP molecule these modes are calculated at 3065, 3050, 3032 and 3011 cm^{-1}. These modes are assigned to a broad band

Table 2 — Potential Energy Distribution and Vibrational Wave Numbers of DCPP

Calculated (DFT)					
Unscaled	Scaled	IR Intensities (km mol^{-1})	Raman activities ($Å^4$ u^{-1})	EXP. FTIR [6]	Assignment (%PED,internal coordinates having contribution >5% are shown
3283	3135	9.30	10.72	3125	ν(C13H)(99)
3210	3065	4.09	115.37	3063	Pr1[ν(C4H)](93)
3208	3064	1.78	230.39	3063	Ph2[ν(C20H)](81)+Ph2[ν(C19H)](17)
3193	3050	15.87	292.86	3063	Pr1[ν(C2H)](74)+Pr1[ν(C3H)](18)
3192	3049	7.89	128.36	3063	Ph2[ν(C20H)]16()+ Ph2[ν(C19H)](45)+ Ph2[ν(C18H)](38)
3178	3035	2.21	46.75		Ph2[ν(C19H)](37)+ Ph2[ν(C18H)](59)
3175	3032	8.43	122.82		Pr1[ν(C3H)](75)+ Pr1[ν(C2H)](18)
3153	3011	16.03	86.68		Pr1[ν(C1H)](92)
3135	2994	2.06	26.41	3007	ν(C15H)(98)
1728	1688	116.34	14.07	1687	CH[ρ(C13H)](6)+CH[ρ(C15H)](6)+δ(C5C)(8)+ δ(C11O)(8)+ν(C13C)(13)+ν(C11O)(59)
1644	1606	359.38	1815.48	1612	CH[ρ(C17H)](10)+CH[ρ(C13H)](10)+ν(C13C)(37) +ν(C11C)(7)+ν(C10C)(15)
1619	1581	44.57	378.63	1572	CH[ρ(C1H7)](7)+CH[ρ(C4H)](6)+Pr1[δ_{asy}(ring1)](8) Pr1[ν(C4H)](10)+ Pr1[ν(C3H)](24)+ Pr1[ν(C=N)](12)+Pr1[ν(C1H)](12)
1612	1575	36.49	1760.46	1572	CH[ρ(C18H)](9)+Ph2[δ_{asy}(CC)](8)+Ph2[ν(C21C)](9)+ Ph2[ν(C20C)](8)+ Ph2[ν(C18C)](24)+ Ph2[ν(C17C)](10)
1608	1571	34.00	186.70		CH[ρ(C2H)](8)+ CH[ρ(C3H)](6)+ Pr1[δ_{asy}(ring1)](9) + Pr1[ν(C=N)](13)+ Pr1[ν(C4H)](10)+ Pr1[ν(C2C)](28)+ Pr1[ν(C1C)](8)
1586	1549	6.65	258.58		CH[ρ(C20H)](11)+ CH[ρ(C19H)](6)+Ph2[δ_{asy}(CC)](8)+ Ph2[ν(C20C)](11)+ Ph2[ν(C19C)](33)+ Ph2[ν(C17C)](10)+ Ph2[ν(C18C)](7)
1495	1460	2.39	17.72	1443	CH[ρ(C1H7)](35)+ CH[ρ(C4H)](17)+ Pr1[ν(C=N)](18))+ Pr1[ν(C1H)](7)
1476	1443	18.00	215.34	1443	CH[ρ(C20H)](6)+ CH[ρ(C19H)](23)+ CH[ρ(C18H)](23)+ Ph2[ν(C20C)](14)+ Ph2[ν(C17C)](12)+ν(C15C)(6)
1462	1428	9.53	107.76	1407	CH[ρ(C2H)](29)+ CH[ρ(C3H)](22)+ Pr1[ν(C4C)](15)+ Pr1[ν(C=N)](9)+ Pr1[ν(C1C)](6)
1441	1408	76.55	46.41	1407	CH[ρ(C20H)](18)+δ(CC)(9)+ CH[ρ(C17H)](10)+ CH[ρ(C13H)](10)+ Ph2[ν(C21C)](19)+ Ph2[ν(C17C)](8)+ Ph2[ν(C18C)](8)
1369	1337	29.22	136.74	1320	CH[ρ(C13H)](31)CH[ρ(C15H)](34)+Ph2[ν(C21C)](6))+ν(C13C) (10)
1345	1314	268.68	215.40		CH[ρ(C15H)](7)+ CH[ρ(C13H)](20)+δ(C11O)(7)+ CH[ρ(C3H)](6)+ν(C15C)(7)+ν(C11C)(12)+ν(C5C)(10)
1316	1286	7.09	34.25		CH[ρ(C1H7)](34)+ CH[ρ(C4H)](9)+ Pr1[ν(C=N)](11)+ Pr1[ν(C4C)](9)
1306	1276	8.58	133.57	1244	Ph2[ν(C21C)](16)+ Ph2[ν(C20C)](12)+ Ph2[ν(C19C)](9)+ Ph2[ν(C18C)](11)+ Ph2[ν(C17C)](20)+ Ph2[ν(C18C)](7)
1300	1270	18.44	51.60	1244	CH[ρ(C13H)](6))+ Pr1[ν(C=N)](14)+ Pr1[ν(C4C)](7)+ Pr1[ν(C3C)](8)+ Pr1[ν(C2C)](8)+ Pr1[ν(C=N)](26)+ Pr1[ν(C1C)](11)
1242	1213	75.01	35.32	1208	CH[ρ(C18H)](7)+Pr1[τ(ring1)](8)+[ν(C5C)](21)+ Pr1[ν(C=N)](8)+ Pr1[ν(C3C)](10)
1222	1194	0.88	96.46	1151	CH[ρ(C18H)](21)+ CH[ρ(C15H)](8)+ CH[ρ(C13H)](14))+ Ph2[ν(C18C)](17)
1206	1178	45.82	111.62	1151	CH[ρ(C20H)](24)+ CH[ρ(C19H)](8)+Ph2[δ_{tri}(CC)](18)+ Ph2[ν(C21C)](15)+ Ph2[ν(C17C)](7)+ Ph2[ν(C18C)](15)
1173	1146	15.97	36.16		CH[ρ(C19H)](36)+ Ph2[ν(C21Cl)](7)+ Ph2[ν(C20C)](12)+ Ph2[ν(C18C)](7)

(*Contd.*)

Table 2 — Potential Energy Distribution and Vibrational Wave Numbers of DCPP (*Contd*.)

Calculated (DFT)					
Unscaled	Scaled	IR Intensities (km mol^{-1})	Raman activities ($Å^4$ u^{-1})	EXP. FTIR [6]	Assignment (%PED,internal coordinates having contribution >5% are shown
1171	1144	4.73	10.68		CH[ρ(C2H)](27)+ CH[ρ(C3H)](30)+ CH[ρ(C4H)](15))+ Pr1[ν(C3C)](6))+ Pr1[ν(C2C)](11)
1126	1100	2.27	3.88	1087	CH[ρ(C20H)](16)+ CH[ρ(C18H)](8)+ Ph2[δ_{tri}(CC)](10)+ Ph2[ν(C22Cl)](6)+ Ph2[ν(C19C)](26)+ Ph2[ν(C18C)](2)
1113	1087	15.59	1.08	1087	CH[ρ(C2H)](24)+ CH[ρ(C4H)](18)+Pr1[τ(ring1)](7)+ Pr1[ν(C3C)](14)+ Pr1[ν(C=N)](7)+ Pr1[ν(C1C)](15)
1068	1043	42.03	27.53	1029	Ph2[δ_{tri}(CC)](20)+ CH[ρ(C4H)](7))+ Ph2[ν(C22Cl)](9)+ν(C11C)(7)+ Pr1[ν(C2C)](11)+ Pr1[ν(C1C)](12)
1064	1039	10.93	26.16	1029	Ph2[δ_{tri}(CC)](22)+ Ph2[ν(C22Cl)](13))+ Ph2[ν(C21C)](6)+ Pr1[ν(C2C)](11)+ Pr1[ν(C1C)](9)
1042	1018	30.81	0.71		δ_{opp}(C17H)(39)+ δ_{opp}(C11H)(14)+τ(C13C)(40)
1040	1016	177.75	202.61		CH[ρ(C13H)](7)+δ(C11O)(10)+Pr1[puck](11))+ ν(C11C)(39)+ Pr1[ν(C4C)](8)+ Pr1[ν(C2C)](6)
1023	999	0.06	0.19	984	Pr1[δ_{opp}(C3H)](14)+ Pr1[δ_{opp}(C4H)](43)+ Pr1[δ_{opp}(C5H)](28)+ Pr1[puck](11)
1014	991	13.74	54.40	984	Pr1[puck](57)+ Pr1[ν(C=N)](12)+ Pr1[ν(C4C)](7)+ Pr1[ν(C=N)](10)
989	966	0.39	0.29	955	Pr1[δ_{opp}(C2N)](50)+ Pr1[δ_{opp}(C3H)](24)+ Pr1[δ_{opp}(C5H)](13)+Pr1[τ_{asy}(CC)](6)
987	964	0.04	0.29		Ph2[δ_{opp}(CC)](16)+ Ph2[δ_{opp}(CC)](48)+ Ph2[δ_{opp}(CC)](22)+Ph2[puck](9)
951	929	24.61	17.57		Ph2[δ_{tri}(CC)](21)+ CH[ρ(C13H)](7)+?+ CH[ρ(C15H)](9))+ Ph2[ν(C21Cl)](12)+ Ph2[ν(C17C)](6)+ ν(C15C)(10)
938	916	0.46	4.33	906	Ph2[δ_{opp}(CC)](10)+ Ph2[δ_{opp}(CC)](13)+ δ_{opp}(C17H)(13)+ δ_{opp}(C11H)(27)+ δ_{opp}(C5C)(6)+ Pr1[δ_{opp}(C2N)](6)
927	906	0.93	0.25	906	Ph2[δ_{opp}(CC)](6))+ Ph2[δ_{opp}(CC)](7)+ Pr1[δ_{opp}(C2N)](21)+ Pr1[δ_{opp}(C3H)](12)+ Pr1[δ_{opp}(C4H)](10)+ Pr1[δ_{opp}(C5H)](32)
911	890	0.19	3.37	872	Ph2[δ_{opp}(CC)](32)+ Ph2[δ_{opp}(CC)](28)+ δ_{opp}(C17H)(9)+ δ_{opp}(C11H)(14)
843	824	12.00	3.34		Ph2[δ_{asy}(CC)](9)+ CH[ρ(C15H)](6)+δ(C11O)(12)+ Ph2[ν(C21Cl)](9)+ ν(C15C)(9))+ ν(C11C)(8)+)+ ν(C5C)(11)
827	808	3.71	5.40		δ_{opp}(C5C)(10)+Pr1[δ_{opp}(C4N)](17)+ Pr1[δ_{opp}(C3H)](16))+ Pr1[puck](23)
788	770	76.44	0.01	775	Ph2[δ_{opp}(CC)](23)+ Ph2[δ_{opp}(CC)](20)+ Ph2[δ_{opp}(CC)](20)+ Ph2[puck](14)
759	741	18.00	0.18	740	Pr1[δ_{opp}(C4N)](7)+ Pr1[δ_{opp}(C2N)](14)+ Pr1[δ_{opp}(C3H)](7)+ Pr1[δ_{opp}(C4H)](24)+ Pr1[puck](42)
750	733	11.85	2.74		Ph2[δ_{asy}(CC)](48)+ Ph2[δ_{tri}(CC)](6)+ Ph2[ν(C22Cl)](16)+ Ph2[ν(C21Cl)](18)
722	705	0.05	0.57	713	Ph2[δ_{opp}(CC)](9)+ Ph2[δ_{opp}(CC)](9)+ Ph2[δ_{opp}(CC)](11)+ Ph2[puck](36)+ Pr1[puck](16)
712	696	20.68	1.04	669	Ph2[δ_{asy}(CC)](9)+δ(C11O)(12)+Pr1[δ_{asy}(CC)](24)+ Pr1[δ_{asy}(CC)](26)
687	671	18.92	0.26	669	Ph2[δ_{opp}(CC)](8)+ Ph2[δ_{opp}(CC)](8)+ Ph2[puck](39)+ δ_{opp}(C5C)(12)+ Pr1[puck](15)
634	619	5.99	7.62	607	Pr1[δ_{asy}(CC)](37)+ Pr1[δ_{asy}(CC)](48)
596	582	52.67	0.66		Ph2[δ_{asy}(CC)](35)+ CH[ρ(C13H)](7)+ δ(C11O)(14)+ Ph2[ν(C21C)](6)
565	552	1.20	44.48	548	δ(CC)(28)+ CH[ρ(C13H)](12)+ δ(C5C)(20)+ δ(C11O)(20)+ Ph2[ν(C22Cl)](7)
552	539	0.18	0.175		Ph2[δ_{opp}(CC)](28)+ Ph2[δ_{opp}(CC)](22)+ Ph2[τ_{asy}(CC)](30)+ Ph2[puck](6)

(*Contd*.)

Table 2 — Potential Energy Distribution and Vibrational Wave Numbers of DCPP (*Contd*.)

Calculated (DFT)					
Unscaled	Scaled	IR Intensities (km mol^{-1})	Raman activities (Å^4 u^{-1})	EXP. FTIR [6]	Assignment (%PED,internal coordinates having contribution >5% are shown
521	509	0.05	0.086	486	Ph2[δ_{opp}(CC)](22)+ Ph2[δ_{opp}(CC)](10)+ Ph2[τ_{asy}(CC)](49)
484	473	5.82	6.18	463	Ph2[δ_{asy}(CC)](7)+ δ(C5C)(16)+ δ(C11O)(16)+ δ(C4C)(11)+ δ(C5N)(11)+ Ph2[ν(C22Cl)](17)+ Ph2[ν(C21Cl)](9)+ ν(C5C)(6)
446	446	0.03	0.102		Pr1[δ_{opp}(C4N)](25)+)+ Pr1[δ_{opp}(C3H)](8)+ Pr2[τ_{asy}(CC)](52)
445	446	6.48	8.16		Ph2[δ(ClC)](14)+ Ph2[δ(ClC)](24)+ δ(CC)(15)+ Ph2[δ_{asy}(CC)](6)+ Ph2[ν(C22Cl)](6)+ ν(C5C)(8)
419	419	3.57	5.55		Ph2[δ(ClC)](19)+ Ph2[δ(ClC)](6)+ Ph2[δ_{asy}(CC)](15)+ CH[ρ(C13H)](6)+ δ(C11O)(8)+ Ph2[ν(C21Cl)](22)
413	414	3.78	0.13		Pr1[τ_{asy}(CC)](10)+ Pr1[τ_{asy}(CC)](72)
352	353	0.27	1.95		Ph2[δ(ClC)](9)+ Ph2[δ(ClC)](8)+ Ph2[δ_{asy}(CC)](14)+ δ(C11O)(10)+ δ(C5C)(7)+ δ(C11O)(7)+δ(C4C)(6)+ δ(C5N)(6)+ Pr1[δ_{asy}(CC)](6)+ Ph2[ν(C22Cl)](8)+ Ph2[ν(C21Cl)](7)+ ν(C5C)(7)
300	301	3.04	0.92		Ph2[δ_{opp}(CC)](24)+ Ph2[δ_{opp}(CC)](11)+ Ph2[δ_{opp}(CC)](6)+ Ph2[δ_{opp}(CC)](7)+ Ph2[τ_{asy}(CC)](18)+τ(C13C)(11)
278	279	11.71	0.90		Ph2[δ(ClC)](15)+ Ph2[δ(ClC)](7)+ δ(CC)(7)+ CH[ρ(C13H)](9)+ δ(C4C)(29)+ δ(C5N)(29)
234	235	0.53	1.03		Ph2[δ_{opp}(CC)](11)+ Ph2[δ_{opp}(CC)](27)+ Ph2[δ_{opp}(CC)](9)+ Ph2[τ_{asy}(CC)](38)
230	231	0.16	1.88		Ph2[δ(ClC)](50)+ Ph2[δ(ClC)](39)
199	200	0.70	0.88		Ph2[δ_{asy}(CC)](8)+ CH[ρ(C15H)](20)+ ν(C15C)(17)+ ν(C11C)(9)+ ν(C5C)(10)
187	182	0.29	5.69		τ(C11C)(2)+ τ(C11O)(2)+ Pr1[δ_{opp}(C4N)](14)+ Pr1[δ_{opp}(C5H)](7)+ Pr1[τ_{asy}(CC)](17)+ Pr1[τ_{asy}(CC)](19)
159	160	3.02	1.46		Ph2[δ(ClC)](10)+ δ(CC)(32)+ δ(C5C)(18)+ δ(C11O)(18)+δ(C4C)(25)+ δ(C5N)(25)
136	136	0.06	1.32		Ph2[δ_{opp}(CC)](7)+ Ph2[τ_{asy}(CC)](40)+ δ_{opp}(C17H)(8)+ τ(C13C)(13)+ τ(C11C)(9)+ τ(C11O)(9)
106	107	0.93	0.13		τ(C13C)(13)+ τ(C15H)(13)+ δ_{opp}(C11H)(6)+ τ(C11C)(11)+ τ(C11O)(11)+ δ_{opp}(C5C)(9)+ τ(C4C)(19)+ τ(C5N)(19)+ Pr1[δ_{opp}(C4N)](15)+ Pr1[τ_{asy}(CC)](8)
54	55	2.32	0.65		Ph2[δ_{opp}(CC)](9)+ Ph2[τ_{asy}(CC)](6)+ Ph2[τ_{asy}(CC)](13)+Ph2[puck](9)+ δ_{opp}(C17H)(6)+ τ(C13C)(7)+ τ(C11C)(20)+ τ(C11O)(20)+ δ(C4C)(12)+ δ(C5N)(12)
48	48	0.93	0.68		CH[ρ(C13H)](28)+ CH[ρ(C15H)](20)+ CH[ρ(C15H)](7)+ δ(C5C)(23)+ δ(C11O)(23)
30	30	1.83	1.41		τ(C13C)(13)+ δ_{opp}(C5C)(6)+ τ(C4C)(55)+ τ(C5N)(55)
12	12	1.47	1.34		Ph2[δ_{opp}(CC)](7)+ Ph2[τ_{asy}(CC)](7)+ τ(C13C)(54)+ τ(C15H)(54)+ δ_{opp}(C17H)(14)+ τ(C11C)(8)+ τ(C11O)(8)

Types of vibration: ν stretching; δ deformation (bending), scissoring; δ_{oop} out-of-plane bending; ω wagging; ρ rocking; τ torsion; Puck, Puckering

centered at 3063 cm^{-1} in experimental FTIR spectrum. The CH in-plane bending modes of Pyridine ring are mainly observed at 1581, 1460, 1428, 1144, and 1087 cm^{-1}. These modes can be assigned to IR experimental peaks at 1572, 1443, 1407, 1087 and 1087cm^{-1}respectively. These modes are highly mixed with each other and also with C-C and C-N stretching.

The mixed mode of C-C and C-N stretching and asymmetric deformation of the ring has been calculated at 1213, 1043 and 991 cm^{-1}, these modes correspond to peaks in FTIR spectra at 1208, 1029 and 984cm^{-1}.The out of plane C-H wagging vibrations are calculated at 966, 906, and 741 cm^{-1} and respectively assigned to experimental peaks at 955, 906 and 740 cm^{-1}. Asymmetric deformation of the ring is calculated at 619 cm^{-1} and matches well with peak at 606 cm^{-1}.

3.2.2: Phenyl ring (Ring 2) vibrations

In aromatic compounds[18], the C-H stretching vibrations appear in the region 3100-3000 cm^{-1}. In

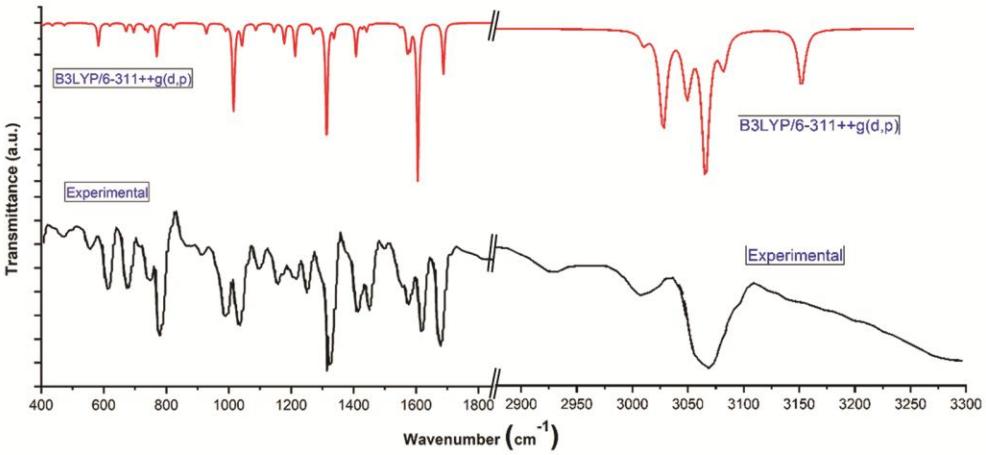

Fig. 2 — Simulated IR spectrum compared with experimental spectrum[6].

DCPP molecule, these modes are calculated at 3064, 3049, 3035 cm^{-1} which is the characteristic region for the ready identification of these vibrations and good match with the observed broad peak at 3063 cm^{-1}. These peaks are also observed in similar range for DPP[3] and CDMA[25] molecules. These bands weakly affected by the substituent group attached to Phenyl ring. The absorption bands arising due to C-H in-plane bending vibrations, mixed with CC stretching vibrations are observed as medium and strong intensity in the region 1614-1161 cm^{-1}. CH in-plane bending modes of the Phenyl ring are calculated at 1606, 1575, 1443, 1337, 1194 and 1178 cm^{-1}. These modes may be assigned to experimental peaks at 1612, 1572, 1443, 1320, and 1151 cm^{-1} respectively. The prominent C-C stretch of the ring are calculated at 1276, 1146 cm^{-1} and may be assigned to nearest observed bands. Out of plane bending vibration of the ring is calculated at 1018 and assigned to observed peak at 1029 cm^{-1}. Torsion of the ring is calculated to be 539 and 509 cm^{-1} and assigned to nearest experimental band at 486 cm^{-1}.

3.2.3: Carbonyl group (C=O) Vibrations

The C=O stretching vibration can be easily identified in the IR due to high degree of conjugation, the strength and the increased polarization. The bonding electrons are not equally distributed between two atoms due to different electron negativities of carbon and oxygen atoms. The lone pair of electrons on oxygen is responsible for the polar nature of carbonyl group. The C=O stretching frequency appears strongly in the IR spectrum in the range 1727 cm^{-1} because of its large change in dipole moment[19]. The carbonyl group vibrations give rise to characteristics bands in vibrational spectra and its characteristic frequency is used to study a wide range of compounds. The intensity of these bands may increase owing to conjugation or formation of hydrogen bonds. The C=O stretching mode has been calculated at 1688 cm^{-1} and very well matches the observed band at 1687 cm^{-1} as an intense peak in FT-IR spectrum.

3.3. Natural bond orbital analysis

Natural bond orbital (NBO) analysis has been done to investigate the intra-molecular interactions and delocalization of the electrons within the molecule. The calculations of natural bond orbital interactions are done using NBO 5.0 program inbuilt in the Gaussian 09 package at DFT/B3LYP/6-311++G(d,p) level of theory. In the NBO analysis[20-21], the electronic wave functions are interpreted in terms of a set of occupied Lewis-type (bond or lone pair) and a set of unoccupied non-Lewis (antibond or Rydberg) localized NBO orbitals. The delocalization effects can be estimated from off-diagonal elements of the Fock matrix in the NBO basis. This is done by analyzing all possible interactions between the filled orbitals of one subsystem and vacant orbitals of another subsystem and estimating their energetic importance. The delocalization effect is measured in terms of interaction energy E(2) value obtained using Kohn–Sham matrix element. The larger the E(2) value, as given in Eq. 1, the more intensive is the interaction between electron donor and electron acceptor, *i.e.* a more donating tendency from electron donors to acceptors and a greater extent of conjugation of the whole system. The charge transfer interactions are formed by the orbital overlap between bonding (π and σ) and antibonding (π^* and σ^*) orbitals which results in intra-molecular charge transfer (ICT) causing

stabilization of the system. The interaction energy E(2) is expressed by the relation

$$E(2) = -n_{\sigma}[\langle\sigma|F|\sigma\rangle^2/(\varepsilon_{\sigma^*} - \varepsilon_{\sigma})] = -n_{\sigma}\left[\frac{F_{ij}^2}{\Delta E}\right]; \quad \ldots (1)$$

Where $n_{\sigma}[\langle\sigma|F|\sigma\rangle^2$ or F^2_{ij} is the Fock matrix element which corresponds to i^{th} and j^{th} NBO orbitals. n_{σ} is the population of the donor σ orbital and ε_{σ^*} and ε_{σ} are the energies of σ* and σ NBOs.

Some important interactions between Lewis and non-Lewis orbitals along with their interacting stabilization energies for DCPP molecule are presented in Table 3. The interaction between electron donors and acceptors becomes more intensive when the value of E(2) becomes large *i.e.* the more electron donating tendency from electron donors to acceptors and the greater the extent of conjugation of the whole system.

Table 3 — Second order perturbation theory analysis of Fock matrix in NBO basis

Donor NBO(i)	ED(i)/e	Acceptor NBO(j)	ED(j)/e	$E^{(2)a}$ kcal mol^{-1}	E(j)-E(i)^b (a.u.)	F(i,j)^c (a.u.)
πC1-C2	1.61722	π*C3-C4	0.27909	20.22	0.29	0.070
		π*C5-N6	0.41826	18.24	0.27	0.063
πC3-C4	1.62641	π*C1-C2	0.29898	18.73	0.28	0.066
		π*C5-N6	0.41826	27.05	0.27	0.077
σC4-H10	1.97754	σ*C5-N6	0.02302	5.53	1.05	0.068
πC5-N6	1.69947	π*C1-C2	0.29898	25.53	0.32	0.081
		π*C3-C4	0.27909	13.27	0.33	0.059
		π*C11-O12	0.18959	12.19	0.33	0.058
πC11-O12	1.96458	π*C5-N6	0.41826	5.38	0.37	0.044
σC11-C13	1.97750	σ*C15-C17	0.02520	5.06	1.11	0.067
πC13-C15	1.82452	π*C11-O12	0.18959	21.12	0.29	0.070
		π*C17-C18	0.37702	11.83	0.29	0.056
σC15-H16	1.97249	σ*C13-H14	0.02080	6.01	0.99	0.069
		σ*C17-C22	0.03888	5.54	1.02	0.067
σC17-C18	1.96323	σ*C22-Cl27	0.02923	5.17	0.84	0.059
πC17-C18	1.61340	π*C13-C15	0.09985	16.36	0.30	0.068
		π*C19-C20	0.32992	20.07	0.28	0.068
		π*C21-C22	0.44106	22.19	0.24	0.067
σC17-C22	1.96880	σ*C21-Cl26	0.02842	8.50	1.88	0.113
πC19-C20	1.64829	π*C17-C18 π*C21-	0.37702	20.82	0.29	0.070
		C22	0.44106	22.29	0.25	0.068
σC21-C22	1.98011	σ*C20-H25	0.01293	5.80	2.23	0.102
πC21-C22	1.70102	π*C17-C18	0.37702	15.72	0.32	0.065
		π*C19-C22	0.32992	17.71	0.31	0.067
σC22-Cl27	1.98754	σ*C20-H25	0.01293	8.99	2.19	0.125
n1(N6)	1.91402	σ*C1-C2	0.02532	8.84	0.90	0.081
		σ*C4-C5	0.03146	9.86	0.90	0.085
n2(O12)	1.88790	σ*C5-C11	0.07473	19.85	0.67	0.104
		σ*C11-C13	0.05971	18.59	0.71	0.104
n3(Cl26)	1.92210	π*C21-C22	0.44106	14.27	0.30	0.065
n3(Cl27)	1.91019	π*C21-C22	0.44106	14.41	0.31	0.065
π*C5-N6	0.41826	π*C1-C2	0.29898	211.27	0.01	0.081
		π*C3-C4	0.27909	176.46	0.02	0.086
		π*C11-O12	0.18959	114.53	0.02	0.074
π*C11-O12	0.18959	π*C13-C15	0.09985	40.48	0.02	0.072
π*C17-C18	0.37702	π*C13-C15	0.09985	66.88	0.02	0.065
π*C21-C22	0.44106	π*C17-C18	0.37702	78.82	0.04	0.080
		π*C19-C20	0.32992	96.76	0.03	0.082

ED is the occupation number.
E(2) is the energy of hyperconjugative interactions.
Eb Energy difference between donor and acceptor i and j NBO orbitals.
F(i, j) is the Fock matrix element between i and j NBO orbitals.

From the Table 3, it is visible that there is a strong intra-molecular hyper conjugative interaction of π electrons between π bond orbitals and anti-bonding orbitals. These interactions are established by the orbital overlapping between π(C–C or C-N) and π*(C–C or C-N) bond orbitals resulting ICT (Intra-molecular charge transfer) which causes stabilization of the system.

In Pyridine ring, a strong delocalization of electron density(ED) is seen among the π(C-C), π (C-N) and π*(C-C), π*(C-N) bonds. These conjugative interactions π(C1-C2) to π*(C3-C4) and π*(C5-N6) with interaction energy 20.22 and 18.24 kcal mol^{-1} respectively, π(C3-C4) to π*(C1-C2) and π*(C5-N6) with interaction energy 18.73 and 27.05 kcal mol^{-1} respectively , π(C5-N6) to π*(C1-C2) and π*(C3-C4) with interaction energy 25.53 and 13.27 kcal mol^{-1} respectively, are identified from the Table 3. This ED transfer from bonding orbital to anti-bonding orbital weakens the bond. Similar type of electron delocalization is also observed in Benzene ring. ED transfer from π(C17-C18) to π*(C13-C15), π*(C19-C20) and π*C21-C22 with stabilization energy 16.36, 20.07 and 22.19 kcal mol^{-1} respectively, from π(C19-C20) to π*(C17-C18) and π*(C21-C22) with stabilization energy 20.82 and 22.29 kcal mol^{-1} respectively and from π(C21-C22) to π*(C17-C18) and π*(C19-C22) with interaction energy 15.72 and 17.71 kcal mol^{-1} respectively is observed for the Benzene ring. These hyperconjugative interactions are mainly responsible for change of character of bonds in both Pyridine and Benzene ring.

The other type of interactions which are evident from Table 3 are (n-π*)and (n-σ*) interactions between a loan pair (LP) and π*and σ* anti-bonding orbitals respectively. These interactions are generally responsible for resonance in the molecule. There are four such interactions n1(N6) to σ*(C1-C2) and σ*C4-C5), n2(O12) to σ*(C5-C11) and σ*(C11-C13), n3(Cl26) to π*(C21-C22), and n3(Cl27) to π*(C21-C22) are observed with interaction energy lying in the range 8.84 -19.85kcal mol^{-1}. Few conjugated σ to σ* interactions are also present with small delocalization energies. Maximum delocalization occurs between π*(C5-N6) to π*(C1-C2), π*(C3-C4), π*(C11-O12) with interaction energies 211.27, 176.46, 114.53 kcal mol^{-1} respectively.

The primary intra-molecular hyper conjugative interaction of n2(O12) distribute to σ*(C5-C11) and σ*(C11-C13) giving the stabilization energy of 19.58 and 18.59 kcal/mol, respectively. This indicates the delocalization of electrons from lone pair orbitals of oxygen atom of CO group to anti bonding electrons on both sides of the carbonyl group. These intra molecular charge transfer interactions (n-σ*, n-π*, π- π*) are mainly responsible for large NLO properties and biological activities such as antimicrobials, anti-inflammatory, anti-fungal, antibiotic and anti-cancer *etc*. This may be understood in terms of ease of polarization of the molecule due to intra-molecular charge transfer.

3.4. Molecular electrostatic potential surface

The molecular electrostatic potential (MEP) surface is a property that the electrons and nuclei of molecule create at each point r in surrounding space. Electrostatic potential helps us to know about the reactivity, hydrogen bonding and structure activity relationship of molecule and match with dipole moment, electron negativity and site of chemical reactivity of the molecule. It also provides us the information of the relative polarity of the molecule. The different values of the electrostatic potential at the surface are represented by different colors; red represents regions of most negative electrostatic potential, blue represents regions of most positive electrostatic potential and green represents regions of zero potential. Fig. 3 shows the pictorial representation of molecular electrostatic potential mapped on the isodensity surface for DCPP molecule calculated at the B3LYP/6-311++G(d,p) level of theory. In Fig. 3, it is clearly visible that red region is concentrated on oxygen atom O12of carbonyl group and also weakly near nitrogen atom N6 of Pyridine ring. These regions have high electron density and

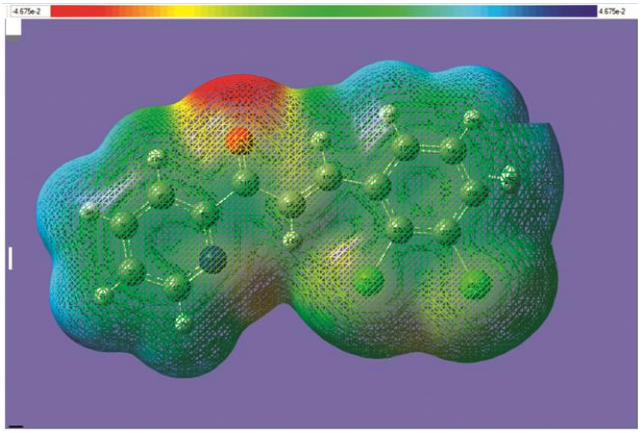

Fig. 3 — Molecular Electrostatic Potential mapped on the isodensity surface for DCPP calculated at the B3LYP/6-311++G(d,p) level of theory.

represent a possible site for electrophilic attack. Similarly, the blue reason is mainly spread over hydrogen atoms of both the rings. These sites are susceptible for nucleophile attack. This picture of MEP shows that molecule is polarized.

3.5. Electronic spectra and HOMO-LUMO analysis

Time-dependent density functional theory (TD-DFT) is a powerful tool for investigating the static and dynamic properties of the molecules in their excited states. UV-Vis spectrum of DCPP molecule was calculated using TD-DFT method[22-23] employing B3LYP/6-311++G(d,p) functional for both gas phase and also in N,N-dimethyl formamide (DMF) solvent. The polarizable continuum model (PCM) was used to include the solvent effect. These calculated spectra is also compared with experimental UV- absorption spectra reported by B. Ganpaya *et al.*[6] in DMF solvent. A comparison of all the three spectra are shown in Fig. 4. The values of wavelength (λ), oscillator strength (f), excitation energies (E) and nature of transitions for calculated spectra compared with experimental peaks wavelength are given in Table 4. Computational spectra for both the medium, air and DMF are showing very good agreement with experimental result. In the DMF solvent four prominent transitions are observed at 338.93, 226.93, 223.23 and 213.45 nm having oscillator strength 0.7813, 0.1592, 0.1379, and 0.3795 respectively. Two intense peaks at 338.93 and 213.45 nm correspond to electronic transition between H→L and H-1→L+3 states. These transitions match well with the experimental peaks at 330 nm and 210 nm respectively. The first transition may be assigned to $n\rightarrow\pi^*$ while the other transition may be assigned to $\pi\rightarrow\pi^*$ transition.

The information about the highest occupied molecular orbital (HOMO) and lowest unoccupied molecular orbital (LUMO) are very important parameters for quantum chemistry. HOMO and LUMO are used to determine the molecular reactivity and the ability of a molecule to absorb light. HOMO, which can be thought as the outer orbital containing electrons, tends to donate these electrons since it is being an electron donor; hence the energy of the HOMO is directly related to the ionization potential. On the other hand, LUMO can be thought as the innermost orbital containing holes to accept electrons; hence LUMO energy is directly related to the electron affinity. The energy gap between the highest occupied and the lowest unoccupied molecular orbital are largely responsible for the chemical and optical properties of the molecules. The 3D surfaces of few frontier orbitals have been drawn and are shown in Fig. 5. These plots can also be used to predict reactive positions in π-electron systems and can explain several types of reactions in conjugated systems. From Fig. 5, it can be seen that HOMO is located on phenyl ring, Ethylene Bridge, and carbonyl group; on the other hand the LUMO is located on entire molecule including pyridine ring. This shows anintramolecular charge transfer during electronic transition. The opposite behavior is visible for HOMO-1 to LUMO+1 transition. Gauss-Sum 2.2

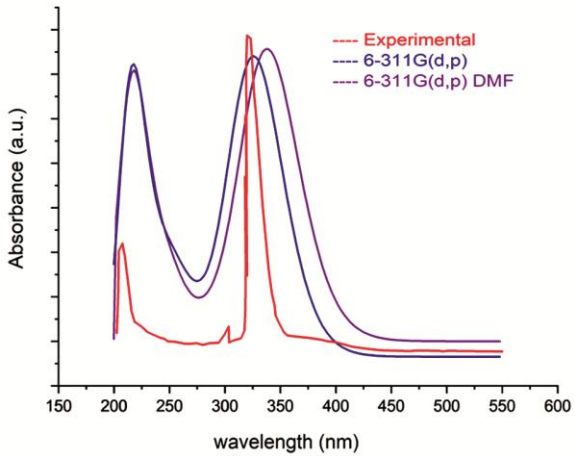

Fig. 4 — Simulated and Experimental UV-Vis spectra of DCPP.

Table 4 — Calculated absorption wavelengths (λ), excitation energies (E) and oscillator strengths (f) of DCPP molecule using TD-DFT method at B3LYP/6-311++G (d, p) level

Phase	Experimental (DMF)[6] λ (nm)	λ (nm)	E (eV)	Oscillator strength (f)	Excitation Transitions		Transition type/ assignments
Gas	-	326.96	3.7920	0.5645	71 → 72 (66%)	H→L	$n\rightarrow\pi^*$
	-	221.07	5.6084	0.1304	68 → 73 (55%)	H-3→L+1	$\pi\rightarrow\pi^*$
	-	218.61	5.6715	0.1029	69→ 74 (62%)	H-2→L+2	$\pi\rightarrow\pi^*$
	-	213.28	5.8133	0.3300	69→ 75 (58%)	H-2→L+3	$\pi\rightarrow\pi^*$
Solvent (DMF)	330	338.93	3.6581	0.7813	71 → 72 (69%)	H→L	$n\rightarrow\pi^*$
	-	226.93	5.4636	0.1592	70 → 73 (62%)	H-1→L+1	$\pi\rightarrow\pi^*$
	210	223.23	5.5541	0.1379	68 → 73 (58%)	H-3→L+1	$\pi\rightarrow\pi^*$
	210	213.45	5.8086	0.3795	70 → 75 (52%)	H-1→L+3	$\pi\rightarrow\pi^*$

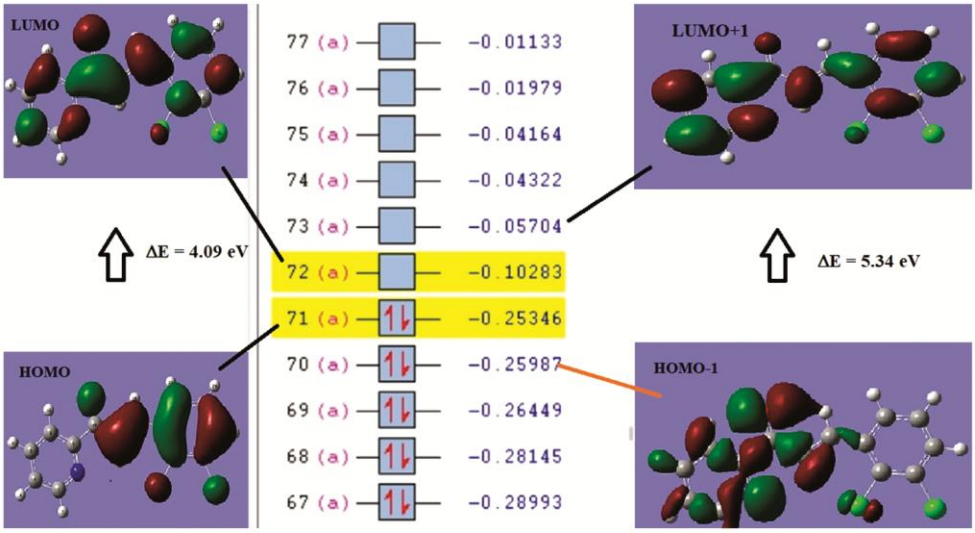

Fig. 5 — HOMO-LUMO plots of DCPP.

Program[24] was used to visualize the total density of the states (TDOS) and the Partial Density of states (PDOS) as shown in Fig. 6. DOS plot shows population analysis per orbital and demonstrates a clear view of the filling up of the molecular orbitals in a certain energy range while PDOS plot shows the percentage contribution of a group to each molecular orbit.

On the basis of HOMO-LUMO energies global reactivity descriptors, such as the energies of frontier molecular orbitals (ε_{HOMO}, ε_{LUMO}), energy band gap ($\varepsilon_{HOMO} - \varepsilon_{LUMO}$), electronegativity ($\chi$), chemical potential ($\mu$), global hardness ($\eta$), global softness (S) and global electrophilicity index (ω), which describe the electrophilic behaviour[25], have been calculated for DCPP molecule using eq (1)-(5):

HOMO energy (B3LYP) = -0.25346 Hartree = -6.897eV

LUMO energy (B3LYP) = -0.10283 Hartree = -2.798eV

Energy band gap ΔE = LUMO – HOMO = 4.09 eV

$\chi = -\frac{1}{2}(\varepsilon_{LUMO}+\varepsilon_{HOMO}) = 0.5157$ eV … (1)

$\mu = -\chi = \frac{1}{2}(\varepsilon_{LUMO}+\varepsilon_{HOMO}) = -0.5157$ eV … (2)

$\eta = \frac{1}{2}(\varepsilon_{LUMO}-\varepsilon_{HOMO}) = 2.045$ eV … (3)

$S = 1/2\eta = 1/4.09 = 0.245$ (eV $^{)-1}$ … (4)

$\omega = \mu^2/2\eta = 0.065$ eV … (5)

3.6 Hyperpolarizability calculations

DFT calculations can be used to explain the nonlinear optical behavior of different type of molecules. The hyperpolarizability calculations play

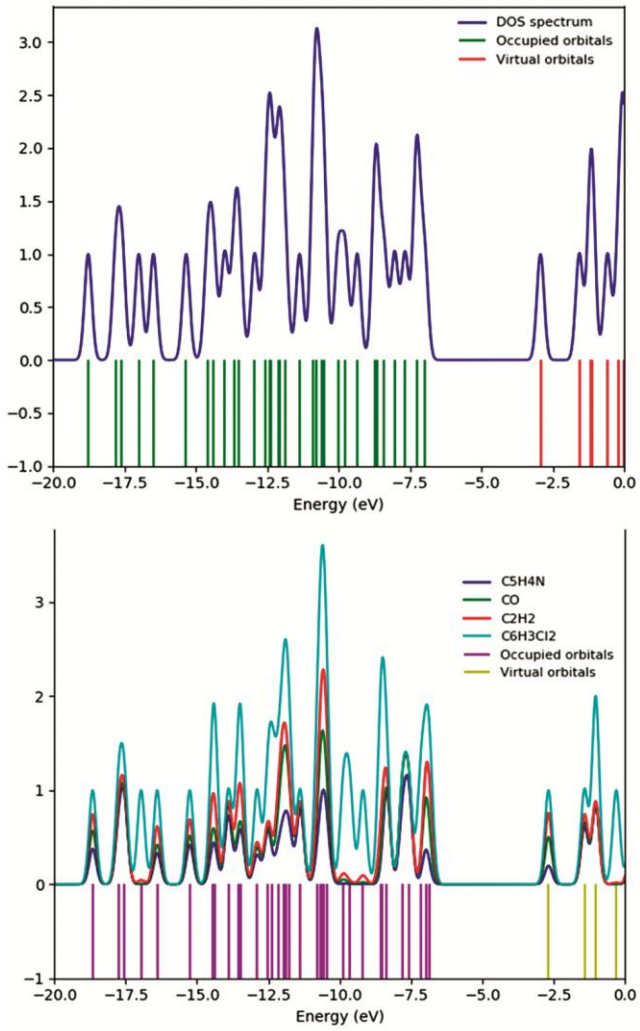

Fig. 6 — DOS and PDOS spectrum of DCPP.

an important role to know the relation between molecular structure and NLO properties. Hyperpolarizability directly shows the NLO behavior of the molecule and is related to the intramolecular charge transfer. The electron cloud can interact with the electric field and due to this it increases the asymmetric electronic distribution in the ground and excited states. First hyperpolarizability β is a third rank tensor that can be described by 3×3× 3 matrices. The 27 components of the 3D matrix can be reduced to 10 components due to the Kleinman symmetry[26]. The components of βare defined as the coefficients in the Taylor series expansion of the energy in the external electric field. When the external electric field is weak and homogeneous, this expansion becomes:

$$E = E^0 - \mu_\alpha F_\alpha - \frac{1}{2}\alpha_{\alpha\beta}F_\alpha F_\beta - \frac{1}{6}\beta_{\alpha\beta\gamma}F_\alpha F_\beta F_\gamma + \quad \ldots (1)$$

Where E^0 is the energy of the unperturbed molecules, $F_\alpha$is the field at the origin, μ_α, $\alpha_{\alpha\beta}$and $\beta_{\alpha\beta\gamma}$ are the components of dipole moment, polarizability and the hyperpolarizability respectively. The total static dipole moment μ, the polarizability α and hyperpolarizability β can be written as their x, y, z components as per the relations given below:

$$\mu = \left(\mu_x^2 + \mu_y^2 + \mu_z^2\right)^{\frac{1}{2}} \quad \ldots (2)$$

$$\alpha = \frac{1}{3}\left(\alpha_{xx} + \alpha_{yy} + \alpha_{zz}\right) \quad \ldots (3)$$

$$\beta_{tot} = [\left(\beta_{xxx} + \beta_{xyy} + \beta_{xzz}\right)^2 + \left(\beta_{yyy} + \beta_{xxy} + \beta_{yzz}\right)^2 + \left(\beta_{zzz} + \beta_{xxz} + \beta_{yyz}\right)^2]^{\frac{1}{2}} \quad \ldots (4)$$

The other important NLO parameter is β_μ which is generally found from electronic field second harmonic generation (EFISH) experiments. It can be calculated by the following relation:

$$\beta_\mu = \frac{\sum_{i=x,y,z}\mu_i(\beta_{ixx}+\beta_{iyy}+\beta_{izz})}{\sqrt{\mu_x^2+\mu_y^2+\mu_z^2}} \quad \ldots (5)$$

The vibrational hyperpolarizability β_μ is used to compare the NLO behavior of the different molecules.

The nonlinear parameters of title molecule are calculated using B3LYP/6-311++G(d,p) method, based on the finite-field approach and are reported in the Table 5

Since the values of the polarizabilities (α) and hyperpolarizability (β) of the Gaussian 09 output are reported in atomic units (a.u.), the calculated values have been converted into electrostatic units (esu) (α: 1 a.u. = 0.1482 × 10^{-24}esu; β: 1 a.u. = 8.3693 × 10^{-33}esu). The value of dipole moment computed using B3LYP/6-311++G(d,p), is 0.4372327a.u or 1.12 D. The polarizability α is calculated equal to 32.46640×10^{-24}esu calculated hyperpolarizability β_{tot} of DCPP is found to be 17.459322×10^{-30}esu which is about 90 times greater than urea(β= 0.1947× 10^{-30} esu)[27]. This higher value of hyperpolarizability β_{tot} confirms that the present molecule DCPP is a potential candidate for Nonlinear Optical applications.

Table 5 — The nonlinear parameters of DCPP molecule calculated using B3LYP/6-311++G(d,p) method

B3LYP/6-311++G(d,p) (a.u)		B3LYP/6-311++G(d,p) (esu * 10^{-24})		B3LYP/6-311++G(d,p) (esu * 10^{-30})	
μ_x	-0.0853356	α_{xx}	35.50870	β_{xxx}	3.679029
μ_y	-0.0001657	α_{xy}	-0.001554	β_{xxy}	-0.000106
μ_z	0.4288447	α_{yy}	14.84668	β_{xyy}	0.482286
μ	0.4372527	α_{xz}	-7.190254	β_{yyy}	-0.001909
		α_{yz}	-0.000504	β_{xxz}	-1.344251
		α_{zz}	47.04384	β_{xyz}	-0.000421
		α	32.46640	β_{yyz}	1.104360
				β_{xzz}	-0.811847
				β_{yzz}	-0.001619
				β_{zzz}	17.374914
				β_{tot}	17.459322

4. Conclusion

A nonlinear optical chalcone derivative: 3-(2,3-dichlorophenyl)-1-(pyridine-2-yl)prop-2-en-1-one (DCPP)was investigated for its structural, spectroscopic, electronic and optical behavior using density functional theory calculations. First of all the geometry of DCPP molecule was optimized using DFT with B3LYP/6-311++G(d,p) basis set. The structural parameters such as bond length, bond angle and torsions were compared with reported experimental data. A satisfactory matching of these parameters were obtained except few torsions which may be associated to isolated molecule model used for calculations, which confirms the validity of our calculations and the basis set used. FTIR spectrum was simulated at the same basis set and a complete potential energy distribution analysis was carried out for quantitative interpretation of observed spectrum. NBO, MEP and HOMO-LUMO studies were reported for understanding the reactive nature and structure–activity relationship of the DCPP molecule.

Finally, the nonlinear optical behavior of this chalcone derivative was studied by calculating dipole moment (μ), polarizability (α) and hyperpolarizability (β) values. The calculated hyperpolarizability β_{tot} of DCPP is 17.459322×10^{-30} esu which is about 90 times greater than urea. This higher value of hyperpolarizability β_{tot} confirms that the present molecule DCPP is a potential candidate for Nonlinear Optical applications.

Acknowledgement

Authors would like to acknowledge the computational facilities provided by the Department of Physics, Chaudhary Charan Singh University, Meerut, during this work. Authors would also like to put on record their sincere thanks to Prof. Beer Pal Singh, HOD Physics for encouragement and fruitful discussions.

References

1 Prabhu A N, Upadhyaya V, Jayarama A & Bhat K S, *Mater Chem Phys*, 138 (2013) 179.
2 Prasad P N & Williams D J, Introduction to Nonlinear Optical Effects in Organic Molecules and Polymers (Wiley, New York), 1991.
3 Yadav M P S, Kumar A & Jayarama A, *Monatsh Chem*, 147 (2016) 1045.
4 Tang Y L, Zheng X, Qi Y, JiaPu X, Liu B, Zhang X, Li X S, Xiao W L, Wan C P & Mao Z W, *Bioorg Chem*, 98 (2020) 1037.
5 Burmaoglu S, Kazancioglu E A, Kaya, R, Kazancioglu M, Karaman M, Algul O & Gulcin I, *J Mol Struct*, 1208 (2020) 127868.
6 Ganapayya B, Jayarama A & Dharmaprakash S M, *Mol Cryst Liquid Cryst*, 571 (2013) 87.
7 Wu D, Zhao B & Zhou Z, *J Mol Struct: THEOCHEM*, 682 (2004) 83.
8 Yadav M P S & Kumar A, *Asian J Phys*, 27 (2018) 23.
9 Frisch M J, Trucks G W, Schlegel H B, Scuseria G E, Robb M A, Cheeseman J R, Scalmani G, Barone V, Mennucci B, Peterson G A, Nakatsuji H, Caricato M, Li X, Hratchian H P, Izmaylov A F, Bloino J, Zheng G, Sonnenberg J L, Hada M, Ehara M, Toyota K, Fukuda R, Hasegawa J, Ishida M, Nakajima T, Honda Y, Kitao O, Nakai H, Vreven T, Montgomery J A, Jr, Peralta J E, Ogliaro F, Bearpark M, Heyd J J, Brothers E, Kudin K N, Staroverov V N, Kobayashi R, Normand J, Raghavachari K, Rendell A, Burant J C, IyengaSr S S, Tomasi J, Cossi M, Rega N, Millam M J, Klene M, Knox J E, Cross J B, Bakken V, Adamo C, Jaramillo J, Gomperts R, Stratmann R E, Yazyev O, Austin A J, Cammi R, Pomeli C, Ochterski J W, Martin R L, Morokuma K, Zakrzewski C G, Voth G A, Salvador P, Dannenberg J J, Dapprich S, Daniels A D, Farkas O, Foresman J B, Ortiz J V, Cioslowski J & Fox D J, Gaussian 09, Revision D.01, Gaussian, Inc Wallingford CT, (2009).
10 Hohenberg P & Kohn W, *Phys Rev B*, 864 (1964) 136.
11 Lee C T, Yang W T & Parr R G, *Phys Rev B*, 37 (1988) 785.
12 Parr R G & Yang W, *Density Functional Theory of Atoms and Molecules*, (Oxford University Press, New York) 1989.
13 Becke A D, *J Chem Phys*, 98 (1993) 5648.
14 Pulay P, Fogarasi G, Pang F & Boggs J E, *J Am Chem Soc*, 101 (10) (1979) 2550.
15 Fogarasi G, Zhou X, Taylor P W & Pulay P, *J Am Chem Soc*, 114 (1992) 8191.
16 Martin J M L & Van A C, Gar2ped, University of Antwerp, 1995.
17 Maurya A, Rastogi S, Rouill G, Huisken F & Henning T, *The Astrophys J*, 755 (2012) 120.
18 Smith B, Infrared spectral interpretation, A systematic approach (CRC Press, Washington) 1999.
19 Prabhu A N, Jayarama A, Subrahmanya B K & Upadhyaya V, *J Mol Struct*, 1031 (2013) 79.
20 Reed A E, Curtiss L A & Weinhold F, *Chem Rev*, 88 (1988) 899.
21 Weinhold F & Landis C R, *Chem Educ Res Pract Eur*, 2 (2001) 91.
22 Casida M E & Chong D P, *Recent Developments in Density Functional Theory*, (World Scientific, Singapore), 1 (1995) 155.
23 Casida M E, Casida K C & Salahub D R, *Int J Quantum Chem*, 70 (1998) 933.
24 O' Boyle N M, Tenderholt A L & Langer K M, *J Comput Chem*, 29 (2008) 839.
25 Pathak S, Kumar A & Tandon P, *J Mol Struct* , 981 (2010) 1.
26 Kleinman D A, *Phys Rev*, 126 (1962) 1977.
27 Sebastian S, Sundaraganesan N, Karthikeiyan B & Srinivasan V, *Spectrochim Acta A*, 78 (2011) 590.